TEMPERATURE DEPENDENCE OF CARBON SUPERSATURATION OF FERRITE IN BAINITIC STEELS

F.G. Caballero[1], M.K. Miller[2], C. Garcia-Mateo[1], J. Cornide[1] and M.J. Santofimia[3]

[1] Department of Physical Metallurgy, Centro Nacional de Investigaciones Metalúrgicas (CENIM-CSIC), Avda. Gregorio del Amo, 8. E-28040 Madrid, Spain

[2] Oak Ridge National Laboratory (ORNL), Materials Science and Technology Division; P.O. Box 2008, Oak Ridge, TN 37831-6139, USA

[3] Department of Materials Science and Engineering, Delft University of Technology, Mekelweg 2, 2628 CD, Delft, The Netherlands

Keywords: Steels, bainite, solid state phase transformation, atom probe tomography (APT)

Abstract

The carbon supersaturation of bainitic ferrite was investigated by means of atom probe tomography in three steels with different carbon and silicon contents, to elucidate the effect of transformation temperature and the reaction velocity on the mechanisms controlling bainite formation with and without the interference of cementite precipitation. Results indicated no difference in the growth mechanism over the

temperature range investigated. These results provide new evidence that the bainite transformation is essentially martensitic in nature.

After decades of debate [1] on the mechanism for the formation of bainite, two primary opposing viewpoints have formally evolved. The shear or displacive theory [2,3] states that bainitic ferrite forms by shear and that the transformation is essentially martensitic in nature (i.e., the individual atom movements are less than one interatomic spacing) and proceeds by the formation of sub-units. The ledge-wise or reconstructive theory [4,5] states that bainite is a product of a reconstructive transformation (i.e. the majority of the phase transformations that occur in the solid state take place by thermally activated atom movements) and grows by the migration of growth ledges on the broad faces of the interface.

Today it is accepted that bainite grows via a displacive mechanism [6,7] i.e., as plate-shaped transformation products exhibiting an invariant plane strain surface relief effect. But there is still much discussion on the diffusion or diffusionless nature of bainite. When it is stated that ferrite grows by a displacive mechanism, it does not imply that it is also diffusionless. For instance, Widmanstätten ferrite forms with a displacive, but diffusional, growth mechanism [8].

Therefore, two different explanations about the growth nature of bainitic ferrite in steels are discussed: the diffusionless hypothesis, which states that bainitic ferrite grows without any diffusion of carbon, and carbon supersaturation is subsequently relieved by partitioning to austenite, and/or through carbide precipitation; and the diffusional hypothesis, which states that bainitic ferrite growth is controlled by carbon diffusion,

and not distinctly different in character from Widmanstätten ferrite, with carbide precipitation at the austenite/ferrite boundaries [6,7].

The traditional criterion for distinguishing between the two bainite transformation theories is whether the newly-formed bainitic ferrite has the para-equilibrium (PE) carbon content or if it is super-saturated in carbon. However, in most alloys, it is impossible to experimentally estimate the initial carbon content of bainitic ferrite since the time taken for any carbon to diffuse into austenite can be extremely short. Carbon resides on interstitial sites in the crystal lattice because its atomic size is sufficiently small relative to that of iron and it can be very mobile even at low temperatures [9].

Recently, the extremely slow transformation kinetics of a nanocrystalline bainitic steel transforming at abnormally low temperatures (200 ºC) allowed for experimental measurements, which demonstrated that bainitic ferrite grows with a high supersaturation of carbon [10]. Results indicated that iron and substitutional atoms, such as Mn, Cr, and Si, do not diffuse during the bainite transformation, but the partitioning of carbon into the residual austenite occurs immediately after formation [10]. The bainite reaction ceases well before the austenite carbon content reaches PE. All these results were explained in terms of the diffusionless growth of bainite sub-units. In addition, atom probe tomography (APT) revealed the presence of a high level of carbon in bainitic ferrite, which was well above that expected from PE with austenite once the reaction proceeds to completion [11].

The relatively slow reaction rate of bainite has been traditionally used as an argument for the diffusional hypothesis because it seemed likely that a growth process, which is martensitic in nature, should be very rapid for trapping carbon in the growing ferrite [12]. In the present work, the carbon content of the bainitic ferrite was analysed by APT

in bainitic steels transformed over a wide range of temperatures (200-525 ºC) to elucidate the role of reaction rate and diffusion in the formation of bainite with and without cementite precipitation.

Three steels with different carbon and silicon contents were selected to evaluate the effect of transformation temperature on carbon supersaturation of ferrite in bainitic steels with and without the interference of cementite precipitation during bainite formation. The bainite transformation temperature range of the steel is mainly a consequence of the carbon content, whereas the inhibition of cementite precipitation during bainite reaction is controlled by the addition of ~1.5 wt.% Si, which retards the precipitation of cementite from austenite because of its low solubility in the cementite crystal structure. The chemical composition of the studied steels is given in Table 1. Details about the manufacturing processes can be found elsewhere [13-15].

Cylindrical dilatometric test pieces [16] were austenitized (at 1200 ºC for 60 s for MC-LSi steel, at 925 ºC for 300 s for MC-HSi steel and at 1000 ºC for 900 s for HC-HSi steel) and then isothermally transformed at temperatures ranging from 200 to 525 ºC for different times before quenching. Prior austenite grain size (PAGS) was revealed by means of a thermal etching technique [17] and measured by the linear intercept method to be (39 ± 14) μm in MC-LSi steel, (12 ± 5) μm in MC-HSi steel and (49 ± 3) μm in HC-HSi steel).

The martensite start temperatures (M_S) listed in Table 2 were estimated by dilatometry. Conventional metallographic examination by Light Optical Microscopy (LOM) and Scanning Electron Microscopy (SEM) were used to determine the bainite start temperatures (B_S) that are shown in Table 2. A JEOL JEM-2010 Transmission Electron

Microscopy (TEM) was used to examine the carbide distribution, inter-lath and intra-lath, in the bainitic microstructure, and to identify the different morphologies of bainite, upper and lower bainite, respectively. The observation of both inter- and intra-lath carbide distributions in the same bainitic microstructure enabled the transition temperatures (LB_S) from upper to lower bainite listed in Table 2 to be determined.

APT specimens were cut from bulk material and electropolished with the standard double layer and micropolishing methods [18]. Atom probe analyses were performed in the Oak Ridge National Laboratory (ORNL) local electrode atom probes (Cameca Instruments LEAP 2017 and LEAP 4000X HR). The local electrode atom probes were operated in voltage-pulse mode with a specimen temperature of 60 K, a pulse repetition rate of 200 kHz, and a pulse fraction of 0.2.

Overall transformation kinetics data reported elsewhere [19,20] are presented in Fig. 1. These data focus only on the start and finish reaction times to allow for an easier comparison; the start time corresponds to the first stage at which bainite could be detected (estimated fraction 0.01) and the finish time is when the fraction ceases to change. As expected, the time-temperature-transformation (TTT) bainitic curves shown in Fig. 1 are shifted to lower temperatures and longer times as the content of carbon is increased in the steel. In addition, alloying elements such Mn, and to lesser extent Cr, decrease the temperature range where ferrite can form [21].

Examples of TEM images for the different products of transformation identified in the studied steels are shown in Fig. 2. The difference in carbide distribution, intra-lath and inter-lath, respectively, makes the classical nomenclature of upper and lower bainite useful, both in describing the microstructural appearance and in classifying the overall

reaction mechanism. Upper bainitic ferrite (α) itself is free from precipitates, as illustrated in Fig. 2a. In contrast, lower bainitic microstructure with cementite inside the ferrite laths is shown in Fig. 2b. Mixed microstructures of upper and lower bainite can be observed defining the lower bainite start temperature (Table 2). This is because the carbon enrichment of the austenite caused by upper bainite transformation can result in the subsequent formation of lower bainite [22].

Silicon additions can avoid the precipitation of cementite between the laths of bainitic ferrite (i.e., upper bainite is carbide-free in high Si steels). A typical carbide-free bainitic microstructure is displayed in Fig. 2c, where it is possible to observe the subunits of bainitic ferrite with retained austenite (γ) among them. However, Si does not have a significant effect on the precipitation of cementite inside the ferrite laths. Thus, the formation of lower bainite is not inhibited in the MC-HSi steel at temperatures ranging from 325-375 ºC (See LB_S in Table 2).

Remarkably, the image shown in Fig. 2e failed to reveal carbide particles inside the bainitic ferrite after transformation at 300 ºC in the HC-HSi steel, leading to the doubtful hypothesis that upper bainite was formed at this extremely low temperature. After an extensive TEM examination, just a few 20 nm wide and 175 nm long cementite (θ) particles were observed in a thicker bainitic ferrite lath (see also Fig. 2e). The presence of cementite as the lower bainite carbide in the HC-HSi steel was confirmed by APT after isothermal transformation at 200 and 300 ºC [11].

TEM examination also revealed that the growth of bainite is accompanied by the formation of dislocations in and around the bainitic ferrite (see Figs. 2a, 2d, and 2f). As bainitic transformation takes place at a temperature at which the shape change cannot be accommodated elastically, the plastic deformation that is driven by the shape change

causes the accumulation of dislocations, which increase in number as the transformation temperature decreases [23,24].

The carbon contents in ferrite, as determined from APT, after transformation at different temperatures in the three studied steels, are shown in Fig. 3. The APT values are estimated using concentration profiles in selected volumes of ferrite that did not contain any carbon-enriched regions, such as cementite particles, dislocations and boundaries. Examples of 3D carbon atom maps showing the carbon distribution in bainitic ferrite regions in contact with austenite or cementite are reported elsewhere [10,11,25]. These APT results reveal the presence of a significant amount of carbon in bainitic ferrite, which was well above that expected from PE phase boundaries, in microstructures transformed below 350 ºC. Results suggest that bainitic ferrite forms as a supersaturated solution of carbon, in spite of the fact that slow reaction rates had been determined at these temperatures (Fig. 1).

The explanation is that a sheaf of bainite consists of several sub-units and the experimental reaction rate applies to the whole bainite constituent, whereas it is proposed that each sub-unit grows with a velocity high enough to trap the carbon of the parent austenite. The rate of sub-units formed was measured using hot-stage photoemission electron microscopy to be 75 μms^{-1} [26], which is many orders of magnitude larger than that calculated assuming PE at the transformation front (0.083 μms^{-1}) [27]. Therefore, sub-unit growth occurs at a rate much faster than expected from carbon diffusion-controlled growth. The average lengthening rate of a sheaf must be then smaller than that of a sub-unit because of the delay between successive sub-units.

The examination of experimental data from materials treated at 525 ºC down to 200 ºC in Fig. 3 did not show any abrupt change of the carbon content in bainitic ferrite that

could indicate a difference in bainite growth mechanism between high and low temperatures. In addition, there is no essential difference in the observed results between steels that transform to bainite with and without the interference of cementite precipitation. This observation lends strong support for the opinion that the bainitic ferrite grows supersaturated with carbon independent of the transformation temperature and the overall reaction rate.

In summary, significant amounts of carbon in bainitic ferrite, which was well above that expected from para-equilibrium phase boundaries, were clearly observed in microstructures transformed below 350 ºC, confirming that bainitic ferrite forms as a supersaturated solution of carbon in spite of the slow reaction rates that had been determined at these temperatures. As the transformation temperature is increased, carbon diffusion is enhanced, providing an opportunity for the decarburization of the supersaturated ferrite soon after the growth event. The excess carbon may then partition into the residual austenite or precipitate in the ferrite in the form of carbides or carbon clusters. Results did not show any discontinuity on the carbon content in bainitic ferrite that could indicate a difference in bainite growth mechanism between high and low temperatures. This investigation provides strong evidence that the bainite transformation is essentially martensitic in nature.

Research was supported by ORNL's Shared Research Equipment (ShaRE) User Facility, which is sponsored by the Office of Basic Energy Sciences, Scientific User Facilities Division, U.S. Department of Energy. The authors also gratefully acknowledge the support of the Research Fund for Coal and Steel and the Spanish Ministry of Science

and Innovation for funding this research under the contracts RFSR-CT-2008-00022 and MAT2010-15330, respectively. J. Cornide also acknowledges the Spanish Ministry of Science and Innovation for financial support in the form of a PhD research grant (FPI).

References

1. Hillert M. Scripta Mater 2002;47:137.
2. Bhadeshia HKDH, Christian JW. Metall Trans A 1990;21:767.
3. Bhadeshia HKDH, Edmonds DV. Acta Metall 1980;28:1265.
4. Aaronson HI. The proeutectoid ferrite and the proeutectoid cementite reactions, in: Zackary VF, Aaronson HI (Eds). The Decomposition of Austenite by Diffusional Processes. New York: Interscience; 1962.
5. Aaronson HI. The Mechanism of Phase Transformations in Crystalline Solids. London: The Institute of Metals; 1969.
6. Hillert M. Scripta Mater 2002;47:175.
7. Borgenstam A, Hillert M, Agren J. Acta Mater 2009;57:3242.
8. Bhadeshia HKDH. Prog Mater Sci 1985;29:321.
9. Winchell PG, Cohen M. Trans ASM 1962;55:347.
10. Caballero FG, Miller MK, Garcia-Mateo C. Acta Mater 2010;58:2338.
11. Caballero FG, Miller MK, Babu SS, Garcia-Mateo C. Acta Mater 2007;55:381.
12. Ko T, Cottrell SA. J Iron Steel Inst 1952;172:307.
13. Caballero FG, Santofimia MJ, Garcia-Mateo C, Garcia de Andrés C. Mater T JIM 2004;45:3272.

14. Caballero FG, Santofimia MJ, García-Mateo C, Chao J, García de Andrés C. Mater Design 2009;30:2077.
15. Caballero FG, Bhadeshia HKDH. Curr Opin Solid State and Mater Sci 2004;8:251.
16. Garcia de Andres C, Caballero FG, Capdevila C, Alvarez LF. Mater Character 2001;46:389.
17. Garcia de Andres C, Bartolome MJ, Capdevila C, San Martin D, Caballero FG, Lopez V. Mater Character 2001;46:389.
18. Miller MK. Atom Probe Tomography. New York: Kluwer Academic/Plenum Press; 2000.
19. Santofimia MJ, Caballero FG, Capdevila C, Garcia-Mateo C, Garcia de Andres C. Mater T JIM 2006;47:1492.
20. Garcia-Mateo C, Caballero FG, Bhadeshia HKDH. ISIJ Int 2003;43:1821.
21. Caballero FG, Miller MK, Garcia-Mateo C. Mater Sci Technol 2010;26:889.
22. Takahashi M, Bhadeshia HKDH. Mater Sci Technol 1990;6:592.
23. Bhadeshia HKDH, Edmonds DV. Metall Trans A 1979; 10:895.
24. Sandvik BPJ. Metall Trans A 1982;13:777.
25. Caballero FG, Garcia-Mateo C, Santofimia MJ, Miller MK, Garcia de Andres C. Acta Mater 2009;57:8.
26. Bhadeshia HKDH. Kinetics, solute-drag and mechanism of the bainite reaction in steels, In: Marder AR, Goldstein JI (Eds.). Proceedings of an International Conference on Phase Transformations in Ferrous Alloys. Philadelphia: AIME; 1984.
27. Ali A, Bhadeshia HKDH. Mater Sci Technol 1989;5:398.

Table Caption:

Table 1: Chemical composition of studied steels, wt-%. The balance is Fe.

Table 2: Experimental critical transformation temperatures.

Figure Captions:

Fig. 1. Start and finish bainite reaction times as a function of transformation temperature. The start time corresponds to the first stage at which bainite could be detected (estimated fraction 0.01), whereas the finish time is when the bainite fraction ceases to change.

Fig. 2. TEM images of (a) upper bainite (i.e. bainitic ferrite and inter-lath cementite particles) obtained at 500 ºC for 180 s in the MC-LSi steel; (b) lower bainite (i.e. bainitic ferrite and intra-lath cementite particles) obtained at 375 ºC for 180 s in the MC-LSi steel; (c) carbide-free bainite consisting of laths of bainitic ferrite separated by films of retained austenite obtained at 425 ºC for 1800 s in the MC-HSi steel; (d) dislocation debris in microstructure formed at 425 ºC for 1800 s in the MC-HSi steel; (e) bainitic microstructure containing bainitic ferrite, retained austenite and intra-lath cementite particles (see detail) obtained at 300 ºC for 28800 s in the HC-HSi steel; (f) dislocation debris in microstructure formed at 200 ºC for 345600 s in the MC-HSi steel; α is bainitic ferrite, γ is retained austenite, and θ is cementite.

Fig. 3. Carbon content in bainitic ferrite as a function of transformation temperature. The para-equilibrium (PE) phase boundary between ferrite and austenite, and ferrite and cementite were calculated for the studied steels (dashed lines-graph has been enlarged to show more clearly calculated PE values) using commercially available software in combination with the SGSOL-SGTE Solution Database 3.0.

Table 1: Chemical composition of studied steels, wt-%. The balance is Fe.

Steel	C	Si	Mn	Ni	Cr	Mo	V
MC-LSi (at. %)	0.30 (1.38)	0.25 (0.49)	1.22 (1.22)	0.10 (0.09)	0.14 (0.15)	0.03 (0.02)	---
MC-HSi (at. %)	0.29 (1.32)	1.48 (2.87)	2.06 (2.04)	---	0.43 (0.45)	0.27 (0.15)	---
HC-HSi (at. %)	0.98 (4.34)	1.46 (2.76)	1.89 (1.82)	---	1.26 (1.28)	0.26 (0.14)	0.09 (0.09)

Table 2: Experimental critical transformation temperatures

Steel	B_S, ºC	LB_S, ºC	M_S, ºC
MC-LSi	525 ± 12	450 ± 12	342 ± 2
MC-HSi	450 ± 12	400 ± 12	299 ± 8
HC-HSi	335 ± 12	335 ± 12	123 ± 4

B_S bainite start, LB_S lower bainite start and M_S martensite start temperatures

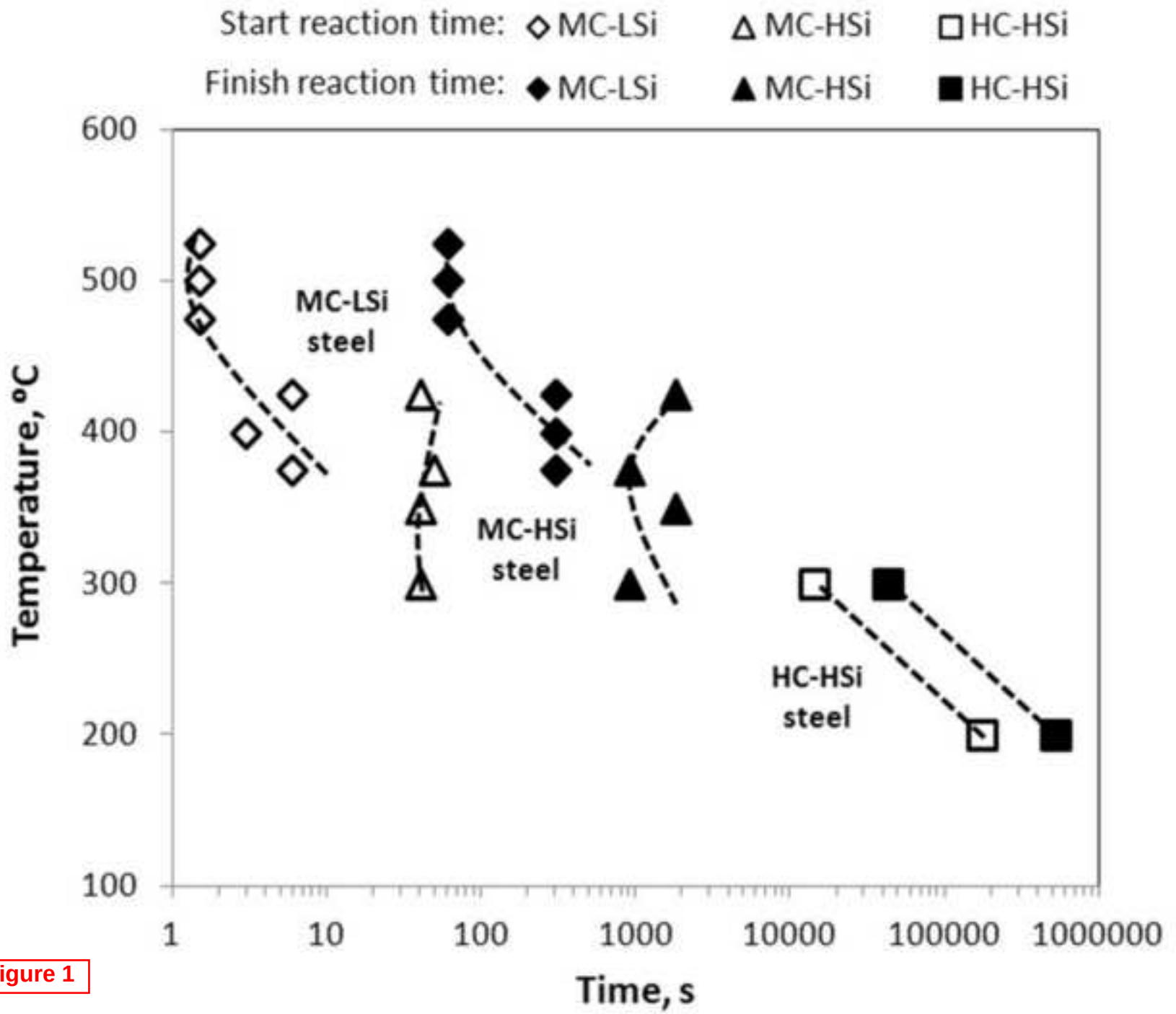
Start reaction time: MC-LSi MC-HSi HC-HSi
Finish reaction time: MC-LSi MC-HSi HC-HSi
600
500
400
300
200
100
Temperature, °C
MC-LSi steel
MC-HSi steel
HC-HSi steel
1
10
100
1000
10000
100000
1000000
Time, s

Figure 1

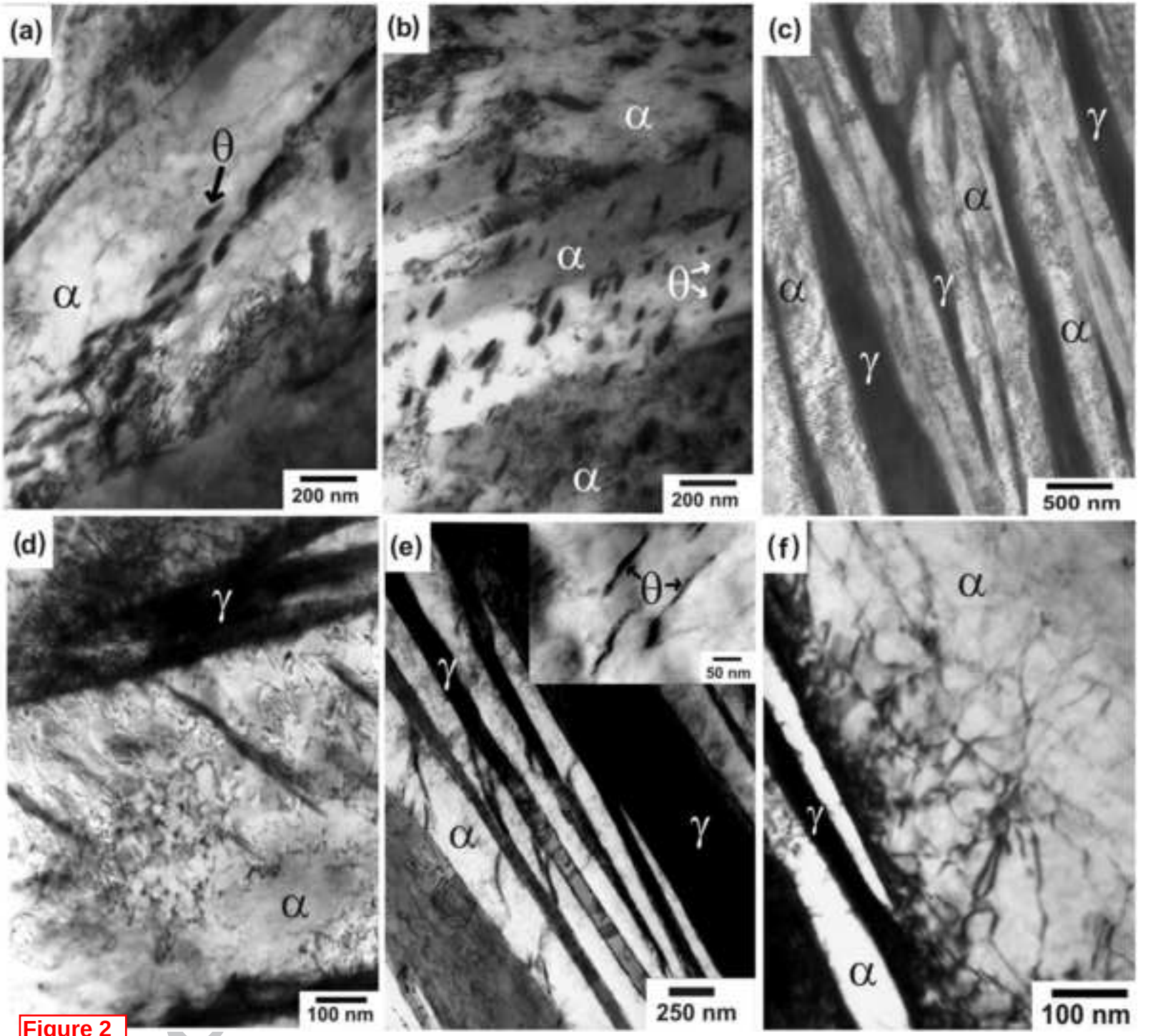
(a)
θ
α
200 nm
(b)
α
α
θ
α
200 nm
(c)
γ
α
α
γ
γ
α
500 nm
(d)
γ
α
100 nm
(e)
θ
50 nm
γ
α
γ
250 nm
(f)
α
γ
α
100 nm

Figure 2

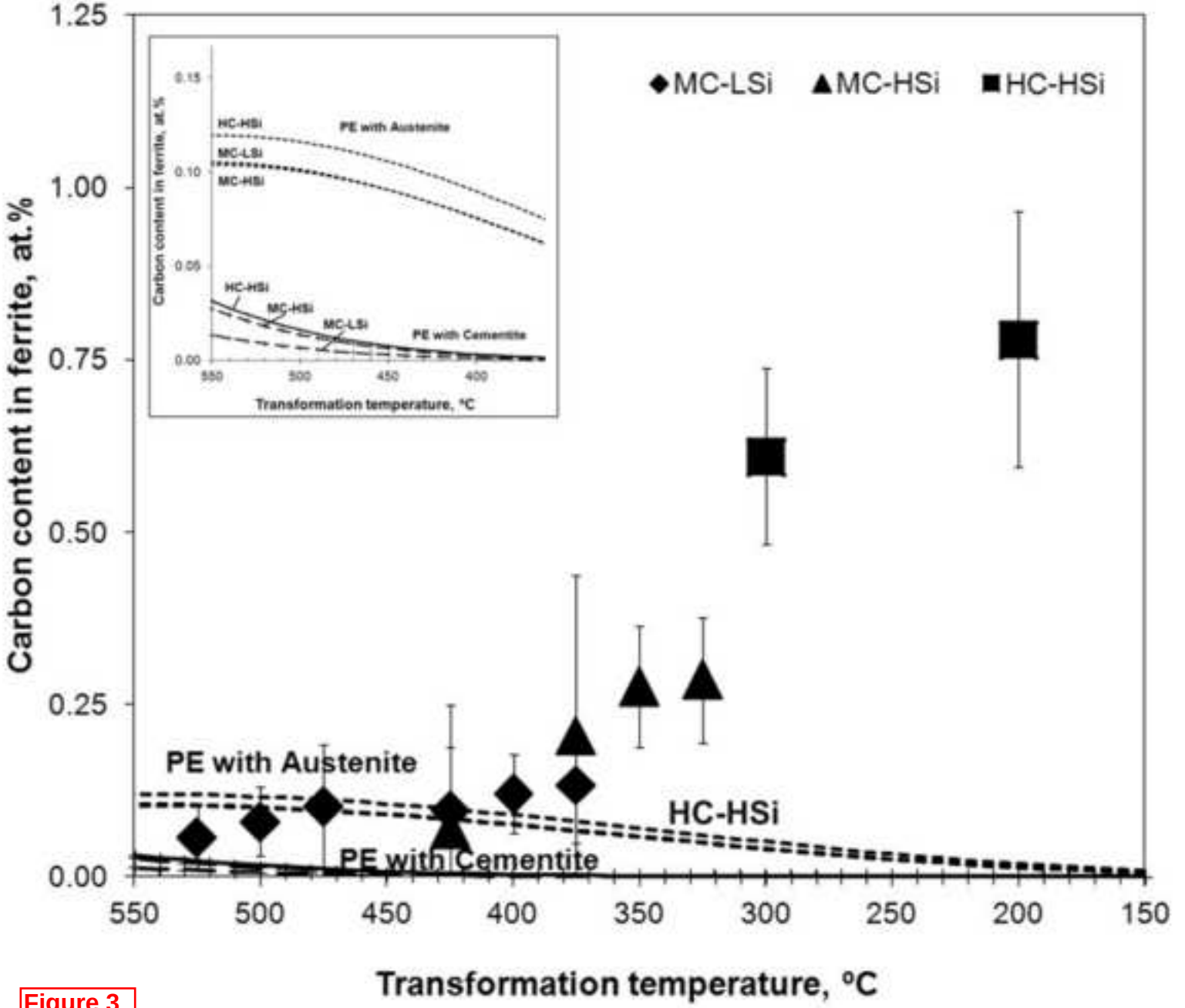
MC-LSi
MC-HSi
HC-HSi
PE with Austenite
HC-HSi
PE with Cementite
Carbon content in ferrite, at.%
Transformation temperature, °C
1.25
1.00
0.75
0.50
0.25
0.00
550
500
450
400
350
300
250
200
150
Carbon content in ferrite, at.%
0.15
0.10
0.05
0.00
HC-HSi
PE with Austenite
MC-LSi
MC-HSi
HC-HSi
MC-HSi
MC-LSi
PE with Cementite
550
500
450
400
Transformation temperature, °C

Figure 3